Local Structure and Short-Range Order in a NiCoCr Solid Solution Alloy

F. X. Zhang, Shijun Zhao, Ke Jin, H. Xue, G. Velisa, H. Bei, R. Huang, J. Y. P. Ko, D. C. Pagan, J. C. Neuefeind, W. J. Weber, and Yanwen Zhang

Phys. Rev. Lett. **118**, 205501 — Published 19 May 2017

DOI: 10.1103/PhysRevLett.118.205501

Local Structure and Short-range Order in a NiCoCr Solid Solution Alloy

F.X. Zhang[1*], Shijun Zhao[1], Ke Jin[1], H. Xue[2], G. Velisa[1], H. Bei[1], R. Huang[3], J.Y.P. Ko[3], D.C. Pagan[3], J.C. Neuefeind[4], W.J. Weber[2,1], Yanwen Zhang[1,2]

[1]*Division of Materials Science and Technology*

Oak Ridge National Laboratory, Oak Ridge, TN 37831, USA

[2]*Department of Materials Science and Engineering, The University of Tennessee,*

Knoxville, TN 37996, USA

[3]*Cornell High Energy Synchrotron Source, Cornell University, Ithaca, NY 14850, USA*

[4]*Spallation Neutron Source, Oak Ridge National Laboratory, Oak Ridge, TN 37831, USA*

Abstract

Multi-element solid solution alloys are intrinsically disordered on the atomic scale, and many of their advanced properties originate from the local structural characteristics. The local structure of a NiCoCr solid solution alloy was measured with X-ray/neutron total scattering and extended X-ray absorption fine structure (EXAFS) techniques. The atomic pair distribution function analysis (PDF) did not exhibit observable structural distortion. However, EXAFS analysis suggested that the Cr atoms were favorably bonded with Ni and Co in the solid solution alloys. This short-range order (SRO) may make an important contribution to the low values of the electrical and thermal conductivities of the Cr-alloyed solid solutions. In addition, EXAFS analysis of Ni ion irradiated samples revealed that the degree of SRO in NiCoCr alloys was enhanced after irradiation.

PACS numbers: 63.50.Gh, 75.40.-s, 72.15.Eb,
**zhangf@ornl.gov*

Unlike conventional alloys, high-entropy alloys (HEAs) are solid solutions with multi principle elements in equal or nearly equiatomic components, and the different atomic species are believed to be randomly distributed in the lattice [1, 2]. As a new class of materials, these compositionally complex alloys have attracted a large number of research interests over the past decade, leading to the discovery of some excellent mechanical properties and interesting physical properties [3-10]. Recently, many multicomponent solid solution alloys with 3*d* transition elements from Cr to Ni in the periodic table, which have similar atomic size, have been synthesized and all of these Ni-based alloys have a simple face-centered cubic (fcc) structure [10-14]. Some of these HEAs exhibit high strength and excellent wear resistance at low and high temperatures, which makes them attractive for industrial applications. For example, five-element solid solution alloy CrMnFeCoNi exhibits damage tolerance with tensile strength above 1 GPa and fracture toughness values exceeding 200 $MPa \cdot m^{-1/2}$, and both strength and ductile improve at cryogenic temperatures [10]. The mechanical strengthening is believed to be caused by the dislocation activities [3,15]. NiCoCr, as the parent alloy with medium-entropy, exhibits one of the highest combinations of strength, ductility and toughness [16]. Due to a lack of chemical periodicity in these solid solution alloys, it is reasonable to expect structural distortions in HEAs. However, the degree of structural distortion of HEAs varies because of the different lattice symmetries and chemical compositions [17-20].

Previous experiments have found that Cr is a specific element in these solid solution alloys that has a critical effect on the mechanical and physical properties [12, 21]. Besides the exceptional damage-tolerance at low temperature, the electrical and thermal conductivity decreased nearly one-order of magnitude for NiCoCr compared with those of NiCo [12]. Due to the multi-principle-element in the fcc structure, a complex local structure is expected in HEAs

which may play an important role to the abnormal mechanical and physical properties of these solid solution alloys. However, local structure characterization is intractable by traditional crystallographic or diffraction methods. Short-range order is not rare in conventional alloys and it has obvious effect on the physical properties and materials performance [22-24]. Due to the chemical complexity, SRO is expected in HEAs and was predicted by density-functional theory recently [25, 26]. However, no direct experimental evidence of SRO in HEAs has been reported. In this paper, the local structure of NiCoCr was characterized by X-ray/neutron total scattering and X-ray absorption measurements, and short-range ordering between atoms of Ni(Co) and Cr was found. By developing a mechanistic theory, Varvenne et al have pointed out that the strengthening of HEAs is mainly due to the dislocation interactions with the random local concentration fluctuations around the average composition [15]. The presence of SRO in HEAs may change the local concentration and dislocation behaviors. The predominance of Ni-Cr and Co-Cr pairs in NiCoCr solid solution call attention for accurate theoretical modellings in order to fully interpret the properties of this type of alloys, as the scenario of totally random alloy structure may be insufficient.

The single phase polycrystal and single crystal samples used for the measurements were synthesized in equal atomic composition from high purity elements (>99.9 pure) by arc melting, casting, zone melting and thermal treatments [12, 16]. The samples were cut into thin disks (~1 mm of thickness for single crystals and ~150 μm for polycrystals) by electrical discharge machining and electrochemically polished. In order to study irradiation effects, samples were implanted with Ni ions in various energies and different doses. The X-ray total scattering measurement was performed at F2 station of CHESS, Cornell University with X-ray energy of 61.332 KeV. The PDF spectrum was obtained by Fourier Transformation of the measured

structure factor in a Q-range of 30 $Å^{-1}$ using software PDFgetX3 [27]. Neutron total scattering was measured with NOMAD beamline at SNS, Oak Ridge National Laboratory in time-of-flight (TOF) mode. Both X-ray and neutron PDF spectra were refined with Rietveld method using PDFGUI software [28]. EXAFS measurement was carried out in fluorescence mode at F3 station of CHESS. In order to measure the very top layer of ion irradiated sample, the sample was tilted to accept only the grazing fluorescent X-rays. The EXAFS spectrum was analyzed with Demeter software [29]. The bond length of different pairs in NiCoCr was calculated with first principal method using the projector augmented wave (PAW) as implemented in the Vienna *ab initio* simulation package (VASP) code [30]. The Perdew-Burke-Ernzerhof exchange-correlation functional was used [31]. The energy cutoff for the plane-wave basis set was 400 eV. All calculations were spin-polarized to take into account the magnetism. A 3×3×3 supercell containing 108 atoms was employed, and the Brilliouin zone was sampled with a 4×4×4 Γ-centered mesh. The alloy was modeled by special quasirandom structures (SQS) [32, 33] through minimizing the Warren-Cowley short range order parameters [22], and the structure was optimized by relaxing the internal coordinates of all atoms at the optimal volume. To investigate the effect of finite temperature on the alloy structure, *ab initio* molecular dynamics simulations were also carried out for the Γ-point with a time step of 2 fs. The total simulation time is around 2.7 ps, and the data over the last 1 ps were averaged to calculate the alloy structures.

Fig.1a shows the X-ray diffraction pattern that is refined with the fcc structure model. In order to detect possible structural distortion, a total scattering measurement was conducted with both TOF neutron and high energy X-ray diffraction measurement for the polycrystal samples. Fig. 1b shows the scattering factor from the TOF neutron measurement in momentum ($Q=4\pi \sin\theta/\lambda$) space. The neutron and X-ray pair distribution function spectra are shown in Fig. 2a. The peak

positions measured using neutron and X-ray scattering are very well in agreement with each other. The intensity of X-ray PDF decays significantly at high Q values because of the lower Q-resolution, and neutron PDF can reach a larger R-range of 50 Å. Again, the PDF spectrum can be well refined with a randomly distributed fcc structure model over the whole range. No obvious lattice distortion is found in NiCoCr solid solution alloys with fcc structure. Rietveld refinement in short radial range of 10 Å results in a good fitting with R_w=0.075, and R_w increases to a reasonable value of 0.096 when the PDF pattern in the whole range (r=50 Å) is fitted. Fig. 2b shows the observed and calculated PDF spectrum for NiCoCr in 20 Å range.

Due to the chemical complexity, NiCoCr solid solution is unlikely to be a perfect fcc structure without lattice distortion. With density functional theory (DFT), local stress of individual atoms in HEAs can be calculated using the locally self-consistent multiple scattering method [34]. Because of very similar atomic size between Ni, Co, Fe, Mn and Cr, the structural distortion in Ni-based fcc solid solution alloys may be very small and cannot be detected directly by total scattering measurement. Previously theoretical calculations [11, 35] did suggest that phonons are more dispersive in the systems with the increase of chemical complexity. Rietveld refinement of the neutron PDF of NiCoCr yields the Debye-Waller factor of 0.0085(2) $Å^2$, which is noticeably larger than that of pure Ni at room temperature (0.0046 $Å^2$ [36]). However, PDF analysis cannot distinguish the bond length and vibrations of pairs between different atomic species because of the very similar atomic size, comparable X-ray/neutron scattering properties. In order to obtain the detailed local structure information in the solid solution alloys, X-ray absorption spectrum was measured at the K-edges of Ni, Co and Cr respectively. Fig. 3 shows the magnitude of the EXAFS function in real space. The first shell peaks around Ni, Co and Cr have a little mismatch, which suggests that the local bond length between different atomic species may be slightly

different. In order to fit the EXAFS function, a cluster with 55 atoms in a fully disordered occupation in the fcc lattice was built based on the Warren-Cowley parameter calculation [22]. Fitting results suggest that the local bond length between Cr and its neighbors is slightly larger than the bond length of Ni and Co with their neighbors. The details of the bond lengths between the core and its nearest neighbor atoms are shown in Table I together with the calculation results. It is interesting that the fitting of EXAFS functions of both Ni and Co K-edges indicated that the bonds of Cr-Ni and Cr-Co have obviously smaller Debye-Waller factors (σ^2) than that of Ni-Co (0.001-0.005 vs 0.008-0.012 $Å^2$). The D-W factor derived from EXAFS corresponds directly to the relative change of bond length, including contributions from both thermal vibration and intrinsic lattice distortion. Smaller D-W factors of Cr-Ni and Cr-Co suggest that Cr is favorably bonded with Ni and Co and forms short-range order in the ternary system. As a result, NiCoCr, while lacking long-range chemical order, is not a fully disordered system. There exists short-range order that Cr atoms have a tendency to separate each other, and more Ni(Co)-Cr pairs exist. EXAFS analysis contains too many parameters in the ternary NiCoCr system, including multi-scattering paths between different atomic species, which limits the spatial resolution. Due to the SRO, NiCoCr can be treated as a pseudo-binary system $(Ni,Co)_2Cr$, which can reduce the uncertainties of EXAFS analysis. The uncertainties of the D-W factors are obviously reduced when NiCoCr is treated as a pseudo-binary system (Table II). The D-W factors of Ni-Cr and Co-Cr are 3 times to one-order of magnitude smaller than that of Ni-Ni(Co) and Co-Co(Ni), and the corresponding atomic displacement is 2-5 times smaller. However, the fitting of the Cr K-edge EXAFS function is not satisfactory with the structure model, and the bond length is 2.54Å for Cr-Ni(Co) and 2.47Å for Cr-Cr. The unreasonable bond lengths are due to the random solid solution structure model. Since Cr has strong tendency to bond with Ni(Co), and Cr is only 1/3 in

the chemical composition, the first shell around Cr will be mainly Ni(Co) atoms even without Cr. If we assume that there is no Cr atoms in the nearest neighbor of Cr, the fitting is much better and a more reasonable bond length for Cr-Ni(Co) (2.507 (8) Å) is derived (Table II).

In Ni-based multicomponent solid solution alloys, different atoms share the same Wyckoff position (*4a*) in the lattice and there is no ordered structure formed. The formation of SRO between different atomic species is due to the intrinsic electron configuration and electronegativities of individual atoms. In the stainless-steel alloys of FeNiCr with different compositions, previous thermal diffuse neutron scattering measurements have revealed [37, 38] that Cr has a strong tendency to bond with Ni forming short-range order. Ni-based multicomponent solid solution alloys have been studied broadly in recent years, and experimental investigations have found that Cr-incorporation in the fcc lattice plays a key role for their physical properties [12]. Generally, both electrical and thermal conductivities decrease with the increase of atomic species in the alloys. However, solid solution alloys with and without Cr-content will have magnitude differences in the transportation properties. The electrical resistant and thermal conductivity of binary NiCo alloy are ~8 μΩ cm and ~70 $Wm^{-1}K^{-1}$, respectively, which change to ~89 μΩ cm and to ~12 $Wm^{-1}K^{-1}$ in NiCoCr ternary system [12]. The same behavior was found in all the other multicomponent alloy systems, and the addition of Cr must have special effect in these alloys. Effects of SRO on the electrical resistivity of alloys have been studied theoretically and experimentally before [24, 26, 39]. For example, resistivity increases by 20-30% with the formation of SRO in NiCu alloys [42], which is not as markedly in NiCoCr compared with binary NiCo. The low values of electrical and thermal conductivity in the Cr-contained alloys are typically considered to be contributed by the strong magnetic/antiferromagnetic effect because the magnetic moment of Cr is anti-parallel with that

of Ni and Co [4]. Short-range-ordering may further enhance this effect due to the existence of Ni-Cr and Co-Cr pairs, and as a result, NiCoCr is paramagnetic down to 5 K [12]. SRO thus makes an important contribution to the significant decrease of the electrical and thermal conductivities of the Cr-alloyed solid solutions.

Cr also has different interesting effects to nuclear alloys, such as improved irradiation performance [11], reduced swelling [40], and reduced radiation-induced ductile-brittle transition temperature [41] by adjusting Cr concentration. All these effects in the alloys originate from the local structures, which may relate to SRO. In FeCr alloy, at increasing Cr concentration to above 11%, Cr atoms tend to clusterize, changing the SRO parameters and its magnetic properties significantly [42]. In NiFeCr ternary alloys, the SRO is different, Cr atoms tend to separate and bond with Ni [37, 38]. Similarly, our study suggests that Cr atoms tend to separate and bond with Ni and Co in NiCoCr alloy.

Due to the intrinsic disordered state, HEAs are expected to be radiation tolerant materials. For example, Granberg et al [43] have explicitly demonstrated that the defect production is much lower in NiCoCr than in elemental Ni after irradiation at room temperature with 1.5 MeV Ni ions. To further investigate the origin of improved radiation resistance in NiCoCr, irradiation experiments using multiple energies of nickel self-ions were carried out on NiCoCr, and subsequently analyzed by PDF and EXAFS measurements. The irradiation was performed at room temperature and the flux is fixed at 2.77×10^{11} cm^{-2} s^{-1}. In order to produce an approximately uniform damage region in a depth of about 3.5 μm, NiCoCr samples were irradiated with Ni ions in energies of 16 MeV, 8 MeV, 4 MeV and 2 MeV, respectively, to different doses in displacements per atoms (dpa) from 0.01 to 1 dpa for the polycrystals and 0.01 to 0.3 dpa for the single crystal samples [44, 45]. At each ion fluence, the local dose was

determined by SRIM calculations [46] using the Kinchen-Pease model under an assumed threshold displacement energy of 40 eV for all elements [11]. The results of the simulations are presented in Fig. 4a, which shows a region of approximately uniform damage to 0.01 dpa to a depth of about 3.5 μm. PDF measurement suggested that both the lattice parameter and atomic displacement (D-W factor) increases with the radiation dose (Fig. 4b). The irradiated NiCoCr samples show slight shift of the first peak in EXAFS spectra (Fig. 4c, Ni K-edge). The fitting results are listed in Table III, and Ni-Cr bond distance slightly decreases from 2.51 Å in virgin to 2.49 Å in 0.3 dpa irradiated single crystal sample, while the corresponding bond length of Ni-Ni(Co) increased by ~0.01 Å. Since the Ni-Cr bond length is slightly smaller than that of Ni-Ni(Co), the above result is an indication that irradiation may enhance the SRO in this alloy and more Ni-Cr pairs formed in the first shell around Ni atoms after ion irradiation. Very recently, in situ TEM analysis has found phase segregation around the dislocation loops in Ni-based solid solution alloys [47, 48] with very high dose of ion and electron irradiation at 500 ˚C. The segregation around the dislocation loops in HEAs observed by TEM may be closely related to the SRO in the alloy. The fluctuation of local chemical composition because of SRO in HEAs will induce non-homogeneous defect formation and growth, and result in segregation under external energy dissipation [47, 48].

In summary, the local structure of NiCoCr was examined with neutron and X-ray pair distribution function analysis and EXAFS measurements. PDF analysis did not show detectable lattice distortion, but EXAFS analysis revealed that Cr in the solid solution alloys has a tendency to bond with Ni and Co and form short-range ordering. This short-range order may make an important contribution to the low values of the electrical and thermal conductivities in the alloy. EXAFS analysis also suggested that SRO is enhanced by ion irradiation in NiCoCr solid solution

alloys, which is related to the observed segregation in the alloys during high dose irradiation at elevated temperature.

Acknowledgment

This work was supported as part of the Energy Dissipation to Defect Evolution (EDDE), an Energy Frontier Research Center funded by the U.S. Department of Energy, Office of Science, Basic Energy of Sciences. Neutron diffraction measurements used resources at the Spallation Neutron Source, a DOE Office of Science User Facility operated by the Oak Ridge National Laboratory. The X-ray PDF and EXAFS measurements were conducted at the Cornell High Energy Synchrotron Source (CHESS) which is supported by the National Science Foundation and the National Institutes of Health/National Institute of General Medical Sciences under NSF award DMR-1332208.

Table I Bond length and Debye-Waller factors of Ni, Co and Cr with their nearest neighbor atoms in NiCoCr alloy from EXAFS measurement fitted with a fully disordered structure model. All the data after "/" are calculated values

	Ni k-edge	Co k-edge	Cr k-edge
R_{Core-A}/cal. (Å)	2.511 (9) /2.501	2.51 (1) /2.492	2.52 (2) /2.502
$\sigma^2_{core-Ni}$ (Å^2)	0.01 (3)	0.01 (4)	0.01 (2)
$\sigma^2_{core-Co}$ (Å^2)	0.01 (4)	0.01 (4)	0.01 (2)
$\sigma^2_{core-Cr}$ (Å^2)	0.002 (2)	0.002 (4)	0.005 (9)

Table II Bond length and Debye-Waller factors of NiCoCr which the EXAFS spectra were fit with a pseudo-binary model of $(Ni,Co)_2Cr$, K-edge of Cr is fitted with a model that no Cr atoms in the nearest neighbor. All the data after "/" are calculated values at 0 K

Ni *k*-edge	Co *k*-edge	Cr *k*-edge
$R_{Ni-Ni(Co)}$: 2.52 (1)/ 2.506 Å	$R_{Co-Co(Ni)}$: 2.54 (1) / 2.498 Å	$R_{Cr-Ni(Co)}$: 2.507 (8) / 2.491 Å
R_{Ni-Cr}: 2.51 (1) / 2.502 Å	R_{Co-Cr}: 2.50 (1) / 2.468 Å	
$\sigma^2_{Ni-Ni(Co)}$: 0.006 (3) Å^2	$\sigma^2_{Co-Co(Ni)}$: 0.012 (4) Å^2	$\sigma^2_{Cr-Ni(Co)}$: 0.004 (2) Å^2
σ^2_{Ni-Cr}: 0.002 (2) Å^2	σ^2_{Co-Cr}: 0.001 (1) Å^2	

Table III Bond length and Debye-Waller factors of NiCoCr irradiated with different dose of Ni ions (measured from Ni K-edge)

	virgin	0.01 dpa	0.03 dpa	0.1 dpa	0.3 dpa
$R_{Ni\text{-}Ni(Co)}$ (Å)	2.52 (1)	2.52 (1)	2.52 (1)	2.53 (1)	2.53 (1)
$R_{Ni\text{-}Cr}$ (Å)	2.51 (1)	2.50 (1)	2.50 (1)	2.49 (2)	2.49 (2)
$\sigma^2_{Ni\text{-}Ni(Co)}$ (Å^2)	0.006 (3)	0.009 (4)	0.008 (2)	0.008 (2)	0.009 (3)
$\sigma^2_{Ni\text{-}Cr}$ (Å^2)	0.002 (2)	0.005 (4)	0.003 (2)	0.002 (1)	0.001 (1)

References

[1] J.W. Yeh, Adv. Eng. Mater. **6,** 299 (2004).
[2] B. Cantor, I.T.H. Chang, P. Knight, A.J.B. Vincent, Mater. Sci. Eng. A **375-377,** 213 (2004).
[3] Z. Zhang, M.M. Mao, J. Wang, B. Gludovatz, Z. Zhang, S.X. Mao, E.P. George, Q. Yu, R.O. Ritchie, Nat. Comms. **6** 10143 (2015).
[4] Y. Zhang, T. Zuo, Z. Tang, M.C. Cao, K.A. Dahmen, P.K. Liaw, Z.P. Lu, Prog. Mater. Sci. **61,** 1 (2013).
[5] Y.J. Zhou, Y. Zhang, Y.L. Wang, G.L. Chen, Appl. Phys. Lett. **90,** 181904 (2007).
[6] C. Lin, H. Tsai, Intermetallics, **19,** 288 (2011).
[7] C. Lu, L. Niu, N. Chen, K. Jin, T. Yang, P. Xiu, Y. Zhang, F. Gao, H. Bei, S. Shi, M.-R. He, I. M. Robertson, W.J. Weber, L.M. Wang, Nat. Commun. 7, 13564 (2016).
[8] Y. Zhang, T. Zuo, Y. Chen, P.K. Liaw, Sci. Rep. **3,** 1455 (2013).
[9] Z. Li, K.G. Pradeep, Y. deng, D. Raabe, C.C. Tasan, Nature, **534,** 227 (2016).
[10] B. Gludovatz, A. Hohenwarter, D. Catoor, E.H. Chang, E.P. George, R.O. Ritchie, Science, **345,** 1153 (2014).
[11] Y. Zhang, G.M. Stocks, K. Jin, C.Y. Lu, H. Bei, B.C. Sales, L. M. Wang, L.K. Beland, R.E. Stoller, G.D. Samolyuk, M. Caro, A. Caro, W.J. Weber, Nat. Comms. **6,** 8736 (2015).
[12] K. Jin, B.C. Sales, G.M. Stocks, G.D. Samolyuk, M. Daene, W.J. Weber, Y. Zhang, H. Bei, Sci. Rep. **6,** 20159 (2016).
[13] M. Laurent-Brocq, A. Akhatova, L. Perriere, S. Chebini, X. Sauvage, E. Leroy, Y. Champion, Acta Mater. **88,** 355 (2015).
[14] O.N. Senkov, J.D. Miller, D.B. Miracle, C. Woodward, Nat. Comm. **6,** 6529 (2015).
[15] C. Varvenne, A. Luque, and W.A. Curtin, Acta Mater. **118,** 164 (2016).
[16] B. Gludovatz, A. Hohenwarter, K.V.S. Thurston, H. Bei, Z. Wu, E.P. George, R.O. Ritchie, Nat. Comms. **7,** 10602 (2016).
[17] L.J. Santodonato, Y. Zhang, M. Feygenson, C.M. Parish, M.C. Cao, R.J.K. Weber, J.C. Neuefeind, Z. Tang, P.K. Liaw, Nat. Comms. **6,** 5964 (2015).
[18] H. Diao, L.J. Santodonato, Z. Tang, T. Egami, P.K. Liaw, JOM **67**, 2321 (2015).
[19] L.R. Owen, E.J. Pickering, H.Y. Playford, H.J. Stone, M.G. Tucker, N.J. Jones, Acta Mater. **122,** 11 (2017).
[20] I. Toda-Caraballo, P.E.J. Rivera-Diaz-del-Castillo, Acta Mater. **71,** 76 (2016).
[21] B.C. Sales, K. Jin, H. Bei, G.M. Stocks, G.D. Samolyuk, A.F. May, M.A. McGurie, Sci. Rep. **6,** 26179 (2016).
[22] J.M. Cowley, Phys. Rev. **77,** 669 (1950).
[23] P.L. Rossiter, P. Wells, J. Phys.C: Solid St.Phys. **4,** 354 (1971).
[24] P.R. Tulip, J.B. Staunton, S. Lowitzer, D. Kodderitzsh, H. Ebert, Phys. Rev. B **77,** 165116 (2008).
[25] P. Singh, A.V. Smirnov, D.D. Johnson, Phys. Rev. B **91,** 224204 (2015).

[26] A. Tamm, A. Aabloo, M. Klintenberg, G. M. Stock, A. Caro, Acta Mater. 99, 307 (2015).
[27] P. Juhás and T. Davis, C.L. Farrow, S.J.L. Billinge, J. Appl. Cryst. **46**, 560-566 (2013).
[28] C.L. Farrow, P. Juhás, J.W. Liu, D. Bryndin, E.S. Bozin, J. Bloch, Th. Proffen, S.J.L. Billinge, J. Phys.: Condens. Mat., **19,** 335219 (2007).
[29] B. Ravel and M. Newville, J. Synch. Rad. **12**, 537 (2005).
[30] G. Kresse and J. Furthmüller, Comput. Mater. Sci., **6,** 15 (1996).
[31] J. P. Perdew, K. Burke and M. Ernzerhof, Phys. Rev. Lett., **77,** 3865 (1996).
[32] M. Methfessel and A. Paxton, Phys. Rev. B, **40,** 3616 (1989).
[33] A. Zunger, S.-H. Wei, L. Ferreira and J. E. Bernard, Phys. Rev. Lett., **65,** 353 (1990).
[34] T. Egami, M. Ojha, O. Khorgolkhuu, D.M. Nicholson, G.M. Stocks, JOM **67,** 2345 (2015).
[35] M. Caro, L.K. Béland, G.D. Samolyuk, R.E. Stoller, A. Caro, J. Alloy Compd., **648,** 408 (2015).
[36] L.M. Peng, G. Ren, S.L. Dudarev, M.J. Whelan, Acta Cryst. A **52,** 456 (1996).
[37] P. Cenedese, F. Bley, S. Lefebvre, Acta Cryst. **A40,** 228 (1984).
[38] A.Z. Menshikov, C. Dimitrov, A.E. Teplykh, J. Phys. III France **7,** 1899 (1997).
[39] Y. Konobeev, A. Dvoriashin, S. Porollo, F. Garner, J. Nucl.Mater. **355,** 124 (2006).
[40] H. Kayano, A. Kimura, M. Narui, Y. Sasaki, Y. Suzuki, S. Ohta, J. Nucl. Mater. **155-157,** 978 (1988).
[41] A. Froideval, R. Iglesias, M. Samaras, S. Schuppler, P. Nagel, D. Grolimund, M. Victoria, W. Hoffelner, Phys. Rev. Lett. **99,** 237201 (2007).
[42] W. Wagner, R. Poerschke, H. Wollenberger, Phil. Mag. **43,** 345 (1981).
[43] F. Granberg, K. Nordlund, M.U. Ullah, K. Jin, C. Lu, H. Bei, L.M. Wang, F. Djurabekova, W.J. Weber and Y. Zhang, Phys. Rev. Lett. **116,** 135504 (2016).
[44] R.J. Olsen, K. Jin, C. Lu, LK. Beland, L. Wang, H. Bei, E.D. Specht, B.C. Larson, J. Nucl. Mat. **469** 153 (2016).
[45] Y. Zhang, M.L. Crespillo, H. Xue, K. Jin, C.H. Chen, C.L. Fontana, J.T. Graham, W.J. Weber, Nucl. Instrum. Method B **338,** 19 (2014).
[46] J.F. Ziegler, M.D. Ziegler, J.P. Biersack, Nucl. Instrum. Method B **268,** 1818 (2010).
[47] C. Lu, T. Yang, K. Jin, N. Gao, P. Xiu, Y. Zhang, F. Gao,H. Bei, W.J. Weber, K. Sun, Y. Dong, L. Wang, Acta Mater. **127,** 98 (2017).
[48] M.-R. He, S. Wang, S. Shi, K. Jin, H. Bei, K. Yasuda, S. Matsumura, K. Higashida, I.M. Robertson, Acta Mater. **126,** 182 (2017).

Figure captions

Fig. 1 (a) XRD pattern of polycrystalline NiCoCr fitted with fcc structure model; (b) Structure factor S(Q) of NiCoCr measured with time-of-flight neutron

Fig. 2 (a) Comparison of the X-ray (red) and neutron (blue) pair distribution function of NiCoCr solid solution alloy in 30 Å range; (b) Rietveld refinement of the neutron PDF profile in 20 Å range (R_w=0.086)

Fig. 3 Magnitude of EXAFS functions measured in the K-edge of Ni, Co and Cr and the slightly difference in the position of the first peak indicates that the bond length of Ni, Co and Cr with its

surround atoms may be different. The Fourier transform of all the k^2-weighted EXAFS functions were conducted in the same k range: 3.0-11.0 $Å^{-1}$.

Fig. 4 (a) Profile of Ni ion irradiation induced damage in NiCoCr predicted using the Kinchon-Pease damage calculation in the SRIM code; (b) Lattice constant and Debye-Waller factor of NiCoCr alloys with different dose of Ni ion irradiation; (b) EXAFS spectrum of single crystal samples irradiated with different dose of Ni ions (k^2-weighted with k range: 3.0-11.0 $Å^{-1}$)

Fig. 1

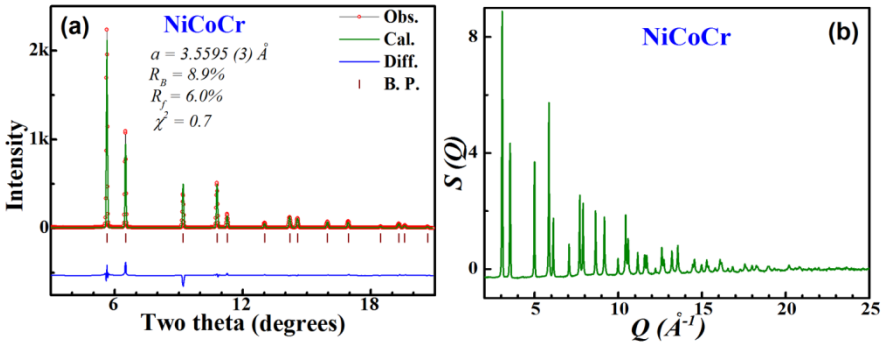

Fig. 2

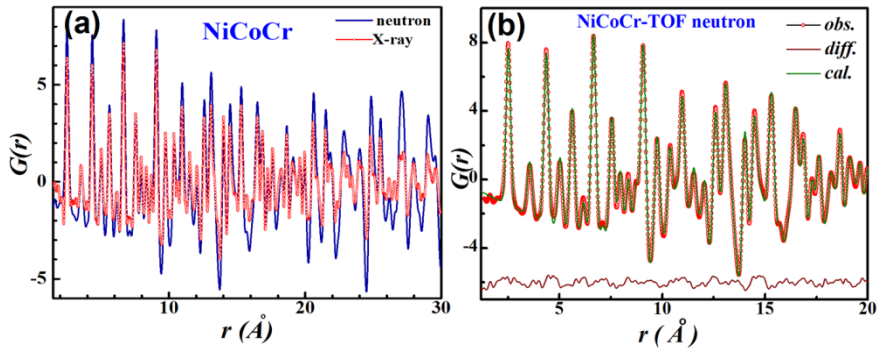

Fig. 3

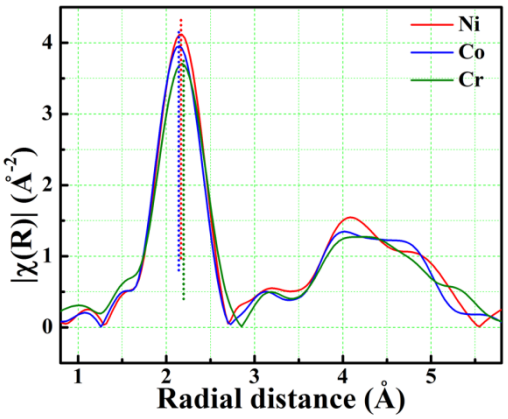
Ni
Co
Cr
|χ(R)| (Å-2)
Radial distance (Å)

Fig. 4

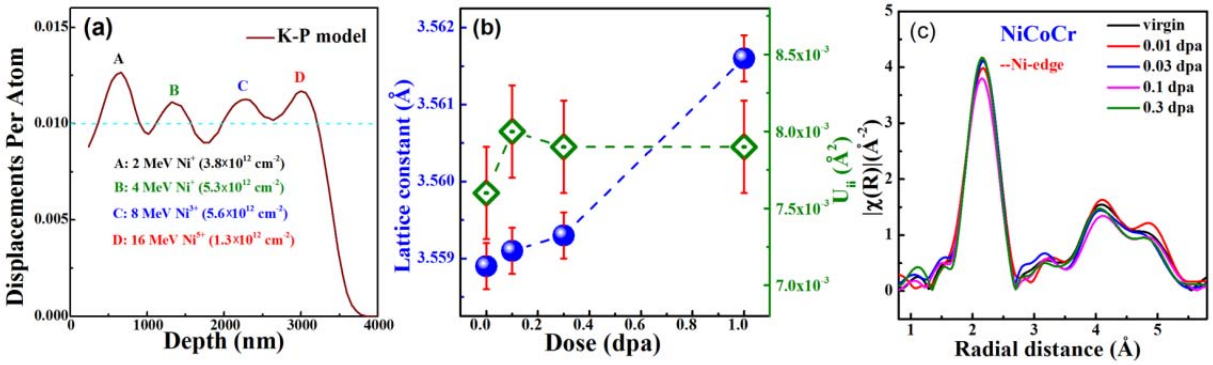
(a)
K-P model
A
B
C
D
A: 2 MeV Ni+ (3.8×10^12 cm-2)
B: 4 MeV Ni+ (5.3×10^12 cm-2)
C: 8 MeV Ni3+ (5.6×10^12 cm-2)
D: 16 MeV Ni5+ (1.3×10^12 cm-2)
Displacements Per Atom
Depth (nm)
(b)
Lattice constant (Å)
Uii (Å2)
Dose (dpa)
(c)
NiCoCr
--Ni-edge
virgin
0.01 dpa
0.03 dpa
0.1 dpa
0.3 dpa
|χ(R)|(Å-2)
Radial distance (Å)